Journal of the European Ceramic Society **17** (1997) 1267–1276

PII: S0955-2219(96)00232-4
0955-2219/97/$17.00

Micromechanisms of Creep-Fatigue Crack Growth in α'-β'-SiAlON at 1200°C

Guo-Dong Zhan, Jian-Lin Shi, Ting-Rong Lai and Tung-Sheng Yen

The State Key Laboratory of High Performance Ceramics and Superfine Microstructure, Shanghai Institute of Ceramics, Shanghai 200050, People's Republic of China

(Received 28 May 1996; revised version received 10 November 1996; accepted 11 November 1996)

Abstract

The cyclic fatigue crack growth characteristics of gas pressure sintered (GPS) Y-α'-β'-Sialon at 1200°C were examined by 'controlled' surface cracking from Vickers indentations in bars loaded in four-point bending. The stress intensity factor for semi-elliptical surface cracks in bending was calculated in terms of the stress and dimensions of the subcritically growing cracks. For comparison, static fatigue crack growth experiments were also carried out on the material. Similar to the fatigue crack growth behaviour of Si_3N_4 at ambient temperature, the high-temperature static and cyclic fatigue crack growth rates showed three characteristic regions having a plateau with a lowest Paris exponent. In the lower stress intensity factor region, cyclic fatigue crack growth rate was slower than that of static fatigue at the same stress intensity factor. In the higher stress intensity factor region, the crack growth rates, both static and cyclic fatigue, were almost the same. Electron microscopy analysis in the crack-tip damage zone indicated that, in addition to the sub-critical crack growth of the main crack assisted by oxidation, creep damage mechanisms such as cavity formation and microcracking may be responsible for static fatigue crack growth in present study. However, it is not significant in the case of cyclic fatigue. Besides, deformation process such as dislocation activity within the matrix grains appeared to play an active role in determining the crack growth kinetics for cyclic loading. It seems that the fatigue stresses will help aid the crystallization process of the amorphous phase and lead to increase the role of dislocation plasticity during high temperature fatigue fracture. © *1997 Elsevier Science Limited.*

1 Introduction

Silicon-nitride-based ceramics are being considered for use in high-temperature structural applications, because of their excellent mechanical property retention and oxidation resistance at high temperatures.[1,2] Designs with successful long-term performance require comprehensive characterization of the mechanical and thermal properties in these materials under a variety of loading conditions at high temperatures, in which fatigue and creep resistance are of major concern. Creep rupture and slow crack growth (SCG) are typical failure mechanisms in ceramics under long-term loading at high temperatures.[3] For creep rupture, failure is usually associated with bulk deformation from extensive nucleation, growth, and coalescence of cavities and microcracks as a result of such creep processes as diffusion or viscous flow. Alternatively, SCG generally occurs by the extension of pre-existing flaws to final, critical sizes, but localized creep damage in the vicinity of the crack tip may occur in the SCG regime under certain conditions. Both creep and SCG processes are time-, temperature- and stress-dependent.[4] Numerous papers have reported the static fatigue and creep rupture behaviour of silicon nitride,[5,6] while limited work has focused on their high-temperature cyclic fatigue properties,[7,8] and even less has been related to the high-temperature cyclic fatigue crack growth behaviour of α'-β'-Sialon ceramics.

In recent years, considerable evidence has been found that monolithic, polycrystalline ceramics and ceramic matrix composites exhibit mechanical fatigue effects at room temperature.[9–23] The fatigue data tend to bear the characteristics of brittle materials: S-N curves are very flat and the exponents in power laws relating crack growth rates to the applied stress intensity factor are very large. In contrast, recent studies on the high-temperature cyclic fatigue behaviour in monolithic, polycrystalline ceramics and ceramic matrix composites such as Si_3N_4, SiC, Al_2O_3, Al_2O_3–SiC, (Mo,W) Si_2–SiC_p composites, have indicated two distinct results (see Ref. 4): (1) apparent 'enhanced' fatigue resistance under cyclic loading compared

to static loading tests under similar test conditions;[7,8,24–30] (2) no true cyclic fatigue effect, as the cyclic fatigue life or cyclic fatigue crack growth rate could be rationalized on the basis of the static loading data.[4] Although some cyclic fatigue data for these materials have been published in the form of stress-life curves,[3,7,8] no attempts were made to rationalize these observations in view of mechanistic explanation from crack growth behaviour in those studies.

The purpose of this experimental study was to characterize cyclic fatigue crack growth behaviour in α'-β'-Sialon. A multiple controlled-indentation technique was used to measure fatigue crack growth rates. Tests are conducted in both static and cyclic tension loading at 1200°C. A direct comparison of static and cyclic fatigue crack growth results will provide some insight into the failure mechanisms in ceramics at high temperatures. Particular attention is paid to the understanding of the micromechanisms of subcritical crack growth using electron microscopy, including scanning electron microscopy (SEM), transmission electron microscopy (TEM), and high resolution transmission electron microscopy (HRTEM) of crack-tip damage. The effects of grain boundary phases in influencing stable crack growth in the present material are also examined.

2 Experimental Procedure

2.1 Material

The starting powders used in this study were Si_3N_4, AlN, Al_2O_3 and Y_2O_3. The mixtures of powders were milled in ethanol for 24 h in an alumina jar, using sintered silicon nitride grinding media. After the powder mixtures were dried, they were die-pressed into bars under 20 MPa and then isostatically pressed under a pressure of 250 MPa. Pressed compacts were placed in a covered graphite crucible with a protective powder bed of 90 wt% Si_3N_4 + 10 wt% BN, and then sintered at 1950°C under 1·5 atm nitrogen pressure for 1 h in a gas pressure sintering furnace. The properties of α'-β'-Sialon ceramic used in this study are shown in Table 1.

2.2 Specimen preparation

Specimens were rectangular bend bars with dimensions of 40 mm × 8 mm × 3 mm. The tensile surface of these specimens was finely ground along the long axis, and then polished using a 1 μm diamond paste to obtain a good finish. A series of Vickers indents was introduced on the tensile surface at different indentation loads. These indents were 1·5 mm apart and carefully aligned so that the corner cracks emanating from the indents were all parallel or perpendicular to the long axis of the specimen.

Four-point bending configuration with an inner span of 10 mm and an outer span of 30 mm was used. Regardless of the contact conditions at these loading points, the linear stress distribution can be accurately determined. This configuration provided data acquisition over a relatively broad range of crack growth from one specimen. For each crack, the initial surface crack length and final length can be recorded. Because these indentation cracks were of various initial lengths, they grew to various lengths during fatigue testing. Thus, there were sufficient crack length data from each test to calculate crack growth rates and stress intensity factors.

2.3 Fatigue tests

Cyclic bending fatigue tests were conducted using a commercial servohydraulic machine (Instron 8501) operated under load control, with a sinusoidal wave form at a frequency of 5 Hz and load ratios R (minimum/maximum loads) of 0·1. The specimen was first heated to 1200°C at a rate of 30°C/min, held for about 30 min in order to relieve indentation residual stress and then slowly loaded until the desired stress level was reached. After a certain time period (predetermined as 20 or 10% of the failure time), the load was removed and the furnace was cooled down. Because the test time was very short, the creep deformation was not considered in our study. The oxide layer on the specimen surface was mildly polished (in the case of the in-air test), and then the surface crack length was measured by a travelling microscope at a magnification of 200×. When the specimen did not fail, a room temperature fracture test was conducted. For comparison, static fatigue tests at the same temperature and maximum stress were also conducted. Following completion of these tests, the fracture surfaces were examined by scanning electron microscope (SEM) in order to measure the size and shape of the initial and the critical cracks. In addition, thin sections were sliced out

Table 1. Properties of α'-β'-Sialon ceramic used in this study

Young's modulus $E(GPa)$	*Hardness* $H_v(GPa)$	*Density* $\rho(g/cm^3)$	*Flexural strength* (MPa)	*Fracture tougness* K_{IC} $(MPa\ m^{1/2})$
300	13·66	3·35	600	5·6

of the fatigue samples for TEM and HRTEM analysis. Circular discs, 3 mm in diameter and 0·1 mm thick, were cut from these slices using an ultrasonic core drill so that the crack tip was located at the center of the disc. These discs were polished, dimpled to approximately 30 μm, and then ion-milled. These perforated samples were investigated under HRTEM, a JEOL 200CX equipped with a top entry double tilt goniometer. In order to ensure that the damage observed in the crack-tip region was caused by high-temperature mechanical loads and not by the TEM specimen preparation techniques, TEM foils were also prepared from the as-received (untested) material, using the same foil preparation techniques, and examined for comparison purposes.

2.4 Data processing

The applied stress intensity factor at the crack tip subject to pure bending was calculated from the finite element analysis of Newman *et al.*[32] for three-dimensional semi-elliptical surface cracks in terms of crack depth, a, half crack length, c, specimen thickness and width, b and t, geometric factors, ϕ and Q, and remote (outer surface) bending stress, σ_a:

$$K_{app} = H\sigma_a(\pi a/Q)^{1/2}F(c/a, c/b, c/t, c/b, \phi) \quad (1)$$

where H is the bending multiplier and F is a geometric function. The aspect ratio, c/a, for the semi-elliptical crack was approximated by using an empirical equation recommended by ASTM E740:[33]

$$a/c = a/b + 1 \quad (2)$$

The indentation fracture mechanics concerning an indentation and its associated elastic-plastic deformation have been developed by Marshall and Lawn.[31] A median crack or Palmqvist crack can be formed by Vickers indentation, depending on the combination of material and stress. Residual stress remains due to plastic deformation. In the case of silicon-nitride-based ceramics, the formation of median cracks is dominant. The residual stress intensity factor, K_r, from the residual crack-opening stress was calculated in terms of indentation load, P, and the half crack length, c, by:[31]

$$K_r = \chi Pc^{-3/2} \quad (3)$$

where the prefactor χ is a material constant, depending on elastic modulus and microhardness. Thus, total stress intensity factor at crack-tip, K_I, for the median crack is given by the summation of eqns (1) and (3), i.e.:

$$K_I = K_{app} + K_r \quad (4)$$

Since most of the residual stress due to indentation had been relieved during heat treatment prior to fatigue loading tests, the applied stress intensity factor was taken as the only driving force for crack advance. Under such a driving force, assume that a time-based fatigue crack growth rate, da/dt, is a function of the stress intensity factor and can be expressed by the equation:

$$da/dt = A\,(K_I)^n \quad (5)$$

where A and n are constants, which can be obtained by least-squares fitting of the measured crack growth data, and K_I is the stress intensity factor at the crack tip. The conventional average method was performed, i.e. the average crack growth rate for each indent was obtained by dividing the total crack extension by test duration, and the average stress intensity factor was the mean value of these stress intensity factors associated with the initial and final crack lengths. For static fatigue, K_I is constant until crack extension. For cyclic fatigue, K_I varies from a minimum (K_{min}) to a maximum (K_{max}) during each cycle. For the latter case, K_I was replaced by K_{max} or ΔK in the present study, that is,

$$da/dN = B\,(K_{max})^m \quad (6)$$

or

$$da/dN = C\,(\Delta K)^m \quad (7)$$

3 Results

3.1 General microstructure features

The X-ray diffraction analysis of the sample indicated the phase compositions of the sample after GPS as α'-Sialon (50 vol%) and β'-Sialon (50 vol%) as the two major crystalline phases, with some grain boundary phases. Figure 1 shows a typical transmission electron micrograph of the multiphase Sialon. α'-Sialon grains are generally equiaxed in shape with an average diameter of 0·45 μm and

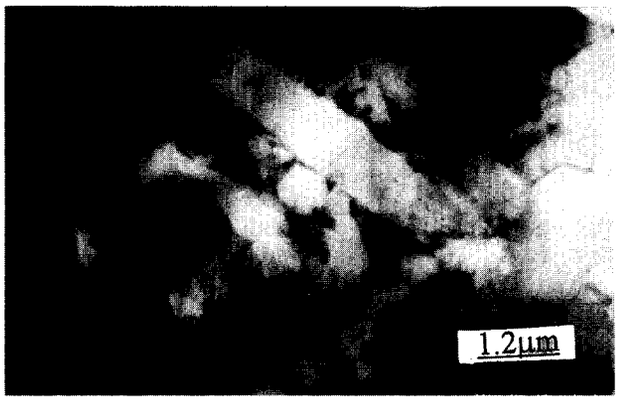

Fig. 1. Microstructure of GPS α'-β'-Sialon showing equiaxed α'-Sialon and elongated β'-Sialon grains.

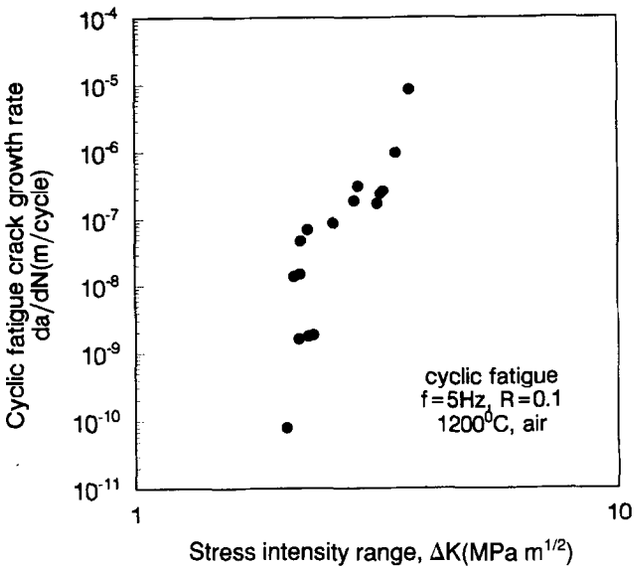

Fig. 2. Relationship between fatigue crack growth rate, *da/dN*, and stress intensity factor range, ΔK for α'-β'-Sialon ceramic composite subjected to cyclic tension loading at 1200°C, cyclic frequency of 5 Hz and load ratio of 0·1.

β'-Sialon grains with an average diameter of 0·65 μm show a whisker-like morphology and the aspect ratio can reach about 3·5.

3.2 High-temperature crack growth behaviour

Figure 2 shows the relationship between fatigue crack growth rate, *da/dN*, and stress intensity factor range, ΔK, for α'-β'-Sialon ceramic composite subjected to cyclic tension loading at 1200°C, cyclic frequency of 5 Hz and load ratio of 0·1. As can been seen from this figure, the cyclic fatigue crack growth behaviour shows three characteristic regions with an almost plateau region at high temperature. However, in 1200°C, in air, the Paris exponent of the composite in the three regions is lower than that at ambient temperature.[10] The Paris exponent m in the plateau region for the composite at 1200°C falls in the same range as that for ductile metals at room temperature (m = 2–4) and some ceramic composites at high temperature (see Table 2). The cyclic fatigue crack growth characteristics of the composite at 1200°C are compared in Fig. 3 with the same trends seen for crack growth under the sustained loads. In order to obtain such a comparison, the cyclic fatigue crack growth per unit time is defined as

$$da/dt = da/dN \times f \tag{8}$$

and the maximum stress intensity factor is given

$$K_{max} = \Delta K/(1 - R) \tag{9}$$

The static fatigue crack growth velocity, *da/dt*, is also plotted in Fig. 3 against the sustained stress intensity factor, K_I. It is interesting to note that several features in Fig. 3 in which are compared crack growth rates at the same K_{max} under both cyclic and static fatigue loading are apparent. First, the cyclic fatigue crack growth per unit time (characterized in terms of K_{max}) is similar to that of static fatigue which has three characteristic regions with an almost flat plateau region. Second, the crack growth retardation due to cyclic fatigue loading is much more pronounced at lower stress intensities; however, the crack growth behaviour under both cyclic and static loading is almost the same at higher stress intensities. Third, the cyclic fatigue crack growth threshold is lower than that of static one. These observations indicate that the crack growth mechanism of high-temperature cyclic fatigue at lower stress intensity is different from that of static fatigue and therefore it is not only time-dependent.

3.3 Microscopic analysis

Figures 4 (a) and (b) are transmission electron micrographs of the fatigue crack-tip regions in

Table 2. Experimental conditions and material parameters for fatigue crack growth for various materials

Material	*Temperature of testing(°C)*	*R*	f*(Hz)*	ΔK *range (MPa m$^{1/2}$)*	*C* (m/cycle(MPa m$^{1/2}$)$^{-m}$)	*m*	*Ref.*
90%pure Al_2O_3	1050	0·15	2·0	2·6–4·8	$6·3 \times 10^{-11}$	8·0	30
Al_2O_3–33 vol% SiC_W	1400	0·15	2·0	3·5–5·5	$4·0 \times 10^{-10}$	3·7	28
Si_3N_4+10 vol% SiC_W	1400	0·1	10	3·0–6·0	$2·6 \times 10^{-13}$	9·13	25
α'-Sialon+β'-Si_3N_4	1400	0·1	0·1	—	$1·8 \times 10^{-11}$	4·25	29
	1400	0·1	1	—	$5·96 \times 10^{-12}$	5·16	29
	1400	0·1	5	—	$2·76 \times 10^{-13}$	8·18	29
(Mo,W)Si2+30 vol% SiC_p +2 wt% C	1300	0·2	10	4·6–7·0	$1·8 \times 10^{-11}$	3·8	26
(Mo,W)Si2+30 vol% SiC_p	1200	0·2	10	4·1–8·0	$3·3 \times 10^{-12}$	3·9	26
	1300	0·2	10	2·1–4·7	$2·3 \times 10^{-10}$	6·0	26
α'-β'-Sialon	1200(region I)	0·1	5	2·06–2·3	$7·13 \times 10^{-17}$	22·0	present study
	1200(region II)	0·1	5	2·3–3·23	$2·33 \times 10^{-9}$	4·01	present study
	1200(region III)	0·1	5	3·23–3·75	$1·3 \times 10^{-21}$	27·6	present study

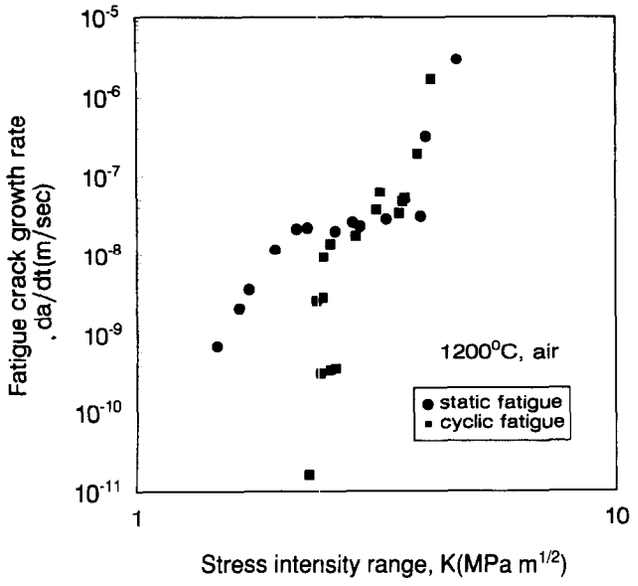

Fig. 3. Variation of crack growth velocity, *da/dt*, as a function of applied stress intensity factor, K, for static crack growth in α'-β'-Sialon ceramic composite at 1200°C in air. Also shown are cyclic fatigue crack growth velocities, $da/dt = (da/dN)xf$, as a function of the maximum stress intensity factor, $K_{max} = \Delta K/(1-R)$, for frequencies $f = 5$ Hz and load ratio, $R = 0{\cdot}1$.

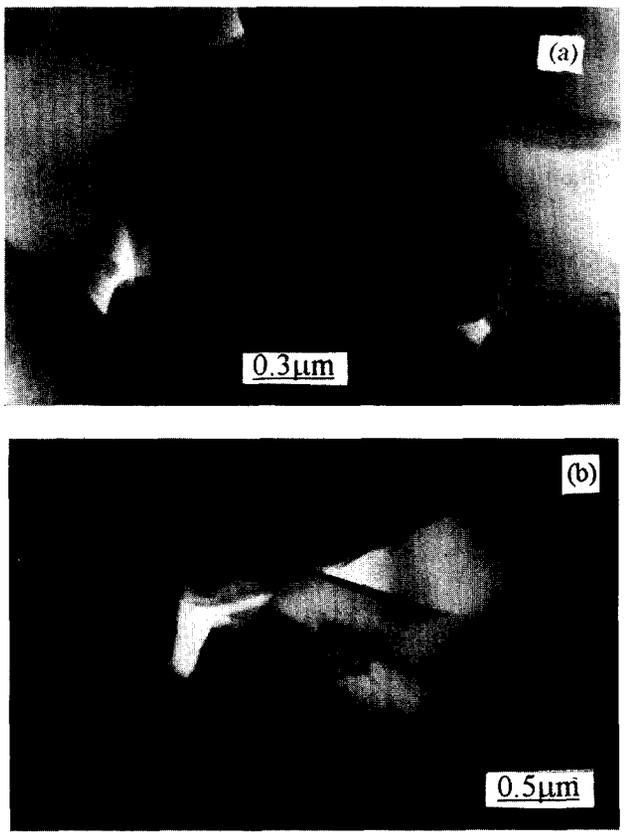

Fig. 4. Transmission electron micrographs of the fatigue crack-tip regions in the ceramic material subjected to a sustained K of 4·5 MPa $m^{1/2}$ in α'-β'-Sialon ceramic composite at 1200°C in air showing (a) extensive cavities at multiple grain junctions and (b) cavity growth along an interface.

the ceramic material subjected to a sustained K of 4·5 MPa $m^{1/2}$ at 1200°C. Extensive cavities at multiple grain junctions can be clearly seen from Fig. 4(a). Cavity growth along an interface is also clearly evident from Fig. 4(b). However, TEM observations of the specimens subjected to cyclic fatigue crack growth experiments at 1200°C showed that the number of such cavities was much smaller than those observed under static fatigue tests. Microcracking was usually observed in the fatigue crack tip subjected to static and cyclic fatigue fracture. Figure 5 is a transmission electron micrograph of the fatigue crack-tip regions in the ceramic material subjected to cyclic fatigue crack growth experiments at $\Delta K = 3{\cdot}5$ MPa $m^{1/2}$ at 1200°C. In this figure, such intergranular microcracking is visible.

Additionally, TEM observations of the specimens subjected to cyclic crack growth tests at $\Delta K = 3{\cdot}0$ MPa $m^{1/2}$ at 1200°C showed that the presence of dislocations within the matrix grains ahead of the fatigue crack tip can be noted (Fig. 6(a)). High resolution transmission electron microscopic observations of crack-tip damage further reinforce the TEM observations. Figure 6(b) is a HRTEM micrograph showing dislocations within the β'-SiAlON [100] grain and having <0001> type Burgers vectors. It cannot be conclusively shown from our present microscopy work whether these dislocations are due to cyclic loading at high temperatures or occur during processing of this material. However, such dislocations have not been observed in the as-received untested material in the present study.

Figure 7 shows the slow crack growth region in the fracture surface of SEM after measuring static fatigue behaviour. As can been seen from this figure, the fracture path of the slow crack growth region was primarily intergranular. Elongated β'-Sialon grains are clearly visible. Also, the fracture mode under cyclic loading was found to

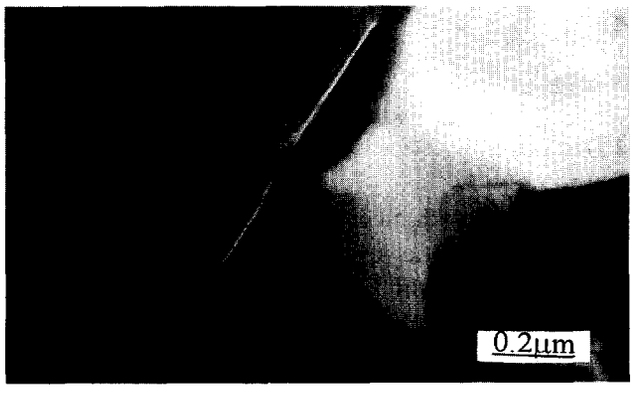

Fig. 5. Transmission electron micrograph of the fatigue crack-tip regions in α'-β'-Sialon ceramic composite subjected to cyclic fatigue crack growth experiments at $\Delta K = 3{\cdot}5$ MPa $m^{1/2}$ at 1200°C showing intergranular microcracking.

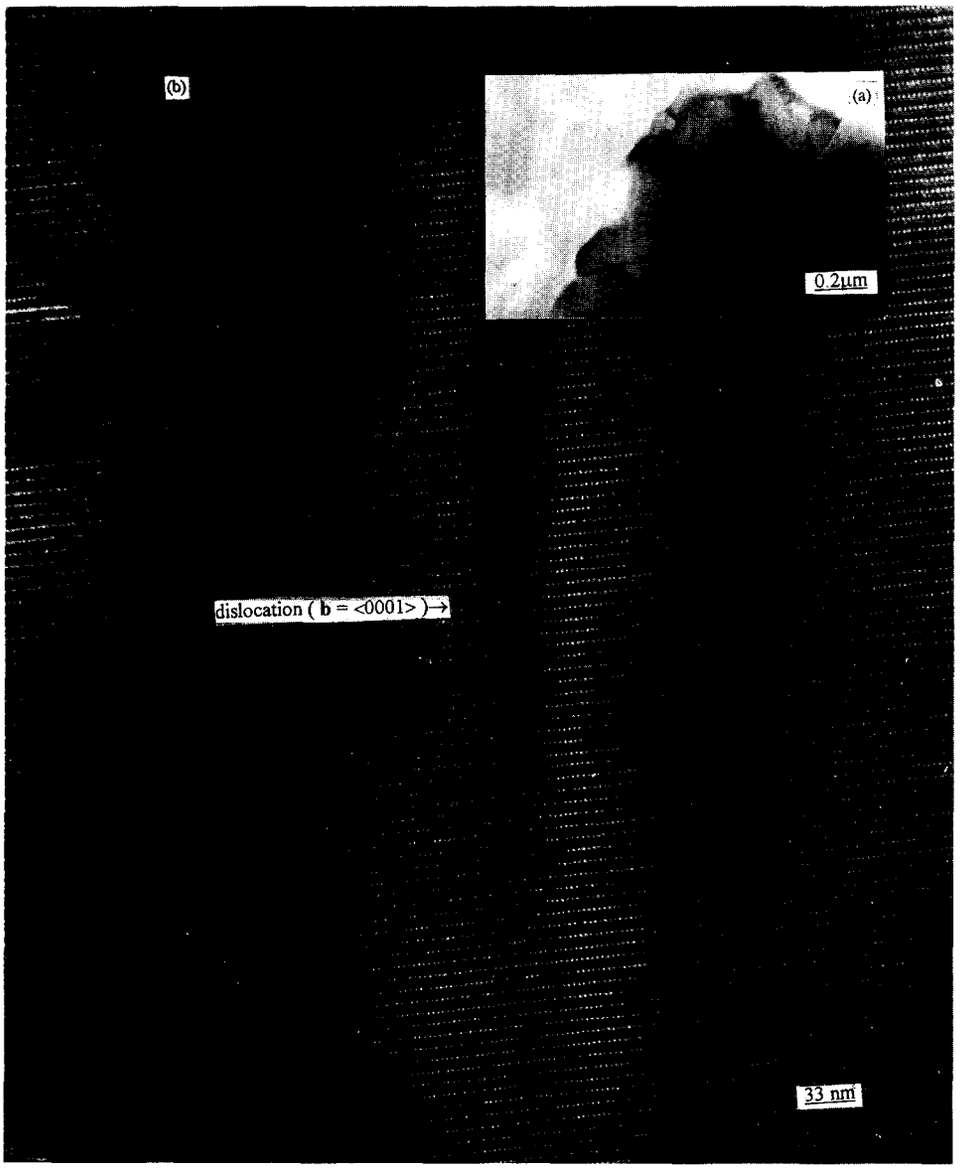

Fig. 6. (a) Transmission electron microscopy micrograph of the specimens subjected to cyclic crack growth tests at $\Delta K = 3{\cdot}0$ MPa $m^{1/2}$ at 1200°C showing the presence of dislocations within the matrix grains ahead of the fatigue crack tip. (b) High resolution transmission electron microscopy (HRTEM) micrograph showing dislocations within the β'-SiAlON [100] grain and having <0001> type Burgers vectors.

be apparently quite similar (Fig. 8). In this figure, enhanced pullout of whisker-like β'-Sialon at high temperature was noted. Besides, some oxidized particles in slow crack growth regions were also visible from Fig. 7 and Fig. 8.

4 Discussion

4.1 Crack growth mechanisms at 1200°C

The above static and low cycle fatigue crack growth behaviour of Y-α'-β'-Sialon with the large elongated β'-Sialon grains at 1200°C in air revealed that slow crack growth was inhibited under cyclic versus static loading in the lower stress intensity factor region. The slower crack growth rate arising from the unloading portion of the cycle may be due to the following reasons.

(a) Pullouts of elongated grains were enhanced during cyclic loading: due to the extremely limited crack tip plasticity in Si_3N_4-based ceramics at room temperature, other nonlinear elastic processes such as frictional sliding of crack wake bridges behind the crack tip have been identified as sources for fatigue degradation.[10] At high temperatures, the fatigue mechanisms may be expected to change. At high temperatures and lower stress intensities, traction of grain boundary sliding is sufficiently reduced to allow much more grain pullouts without grain fracture as shown in Fig. 8. In Y-α'-β'-Sialon made of equiaxed α'-Sialon grains and whisker-like β'-Sialon, bridging of crack faces by many pullouts of whisker-like β'-Sialon grains in the wake of the crack tip can shield the crack tip from the applied stress intensity and the effective stress intensity at crack

Fig. 7. The slow crack growth region in the fracture surface of SEM after measuring static fatigue behaviour. Note that the fracture mode of grains in the slow crack growth was intergranular fracture in equiaxial α'-Sialon crystals and pull-out of whisker-like β'-Sialon.

Fig. 8. SEM fractographic examination of the resulting cyclic fatigue fracture surfaces showing enhanced pullout of whisker-like β'-Sialon at high temperature during the repeated opening and closing of the crack.

tip be somewhat reduced. However, at higher stress intensity factors the chance of breaking grains at the crack tip before their pullout is substantially increased, and leads to reduce the above shielding mechanism of the crack tip. Therefore, the crack growth rates at lower stress intensity factors are slower under cyclic loading than under static loading, and they are almost the same at higher stress intensity factors. This is in agreement with the results of S.-Y. Liu *et al.*[29]

(b) During high-temperature fatigue testing, there were some microvoids or microcracks as well as Vickers indentation damage regions on the tensile surface of the specimen, and oxygen from the atmosphere penetrated into these surface flaws and formed an oxidized layer at the crack tip. The experimental results indicated that the oxidation was more severe under constant opening of the crack tip in static fatigue than under the loading–unloading condition in cyclic fatigue, which in turn caused significant retardation of crack growth in cyclic loading. This is similar to that observed in (Mo,W)Si_2–SiC_p–2%C composite where the addition of carbon to the (Mo,W)Si_2 composite reinforced with 30 vol% SiC particles reduces the content of glass phases and increases its high temperature capabilities by lowering the crack growth rates and increasing the threshold for crack growth initiation.[26]

(c) The reason for the lower crack growth during cyclic fatigue can be also a consequence of the forming of glass bridges and healing effects by the low viscosity grain boundary phase.

4.2 The role of dislocation plasticity at 1200°C

Si_3N_4-based materials are known to undergo a brittle-to-ductile transition at approximately 1000°C.[24] Although the exact mechanism and temperature for this brittle-to-ductile transition in the present material are not clear at present, many studies suggest that it is due to increased dislocation plasticity at high temperatures.[3,4] One of the necessary conditions for stable crack growth is that nonlinear deformation and damage processes exist at the crack-tip region.[4] In metals and alloys, fatigue damage is attributed to irreversible plastic deformation caused by dislocation motion. This process is not considered to be the dominant one for room-temperature fatigue of ceramics. However, it might be plausible for the fatigue of some ceramics at high temperatures where the dislocation motion is active.[25,26] TEM and HRTEM studies in the vicinity of crack tips had shown dislocations within the β'-Sialon grains in specimens subjected to cyclic loads at 1200°C. This dislocation activity may be one of the mechanisms of subcritical crack growth and thus its contribution to nonlinear deformation may not be neglected under cyclic loading. Si_3N_4-based multiphase ceramics densified via liquid-phase sintering have been reported[27] to contain amorphous phases at triple grain junctions and grain boundaries which may described as metal–Al–Si–O–N oxynitride glasses depending on the sintering additive composition. However, it seems that, in addition to temperature, the applied fatigue stresses will help aid the crystallization process of the amorphous phase (Fig. 9). This led to a decrease in the content of glassy phase and the width of the interfacial phase, so that grain boundary sliding became difficult. Consequently,

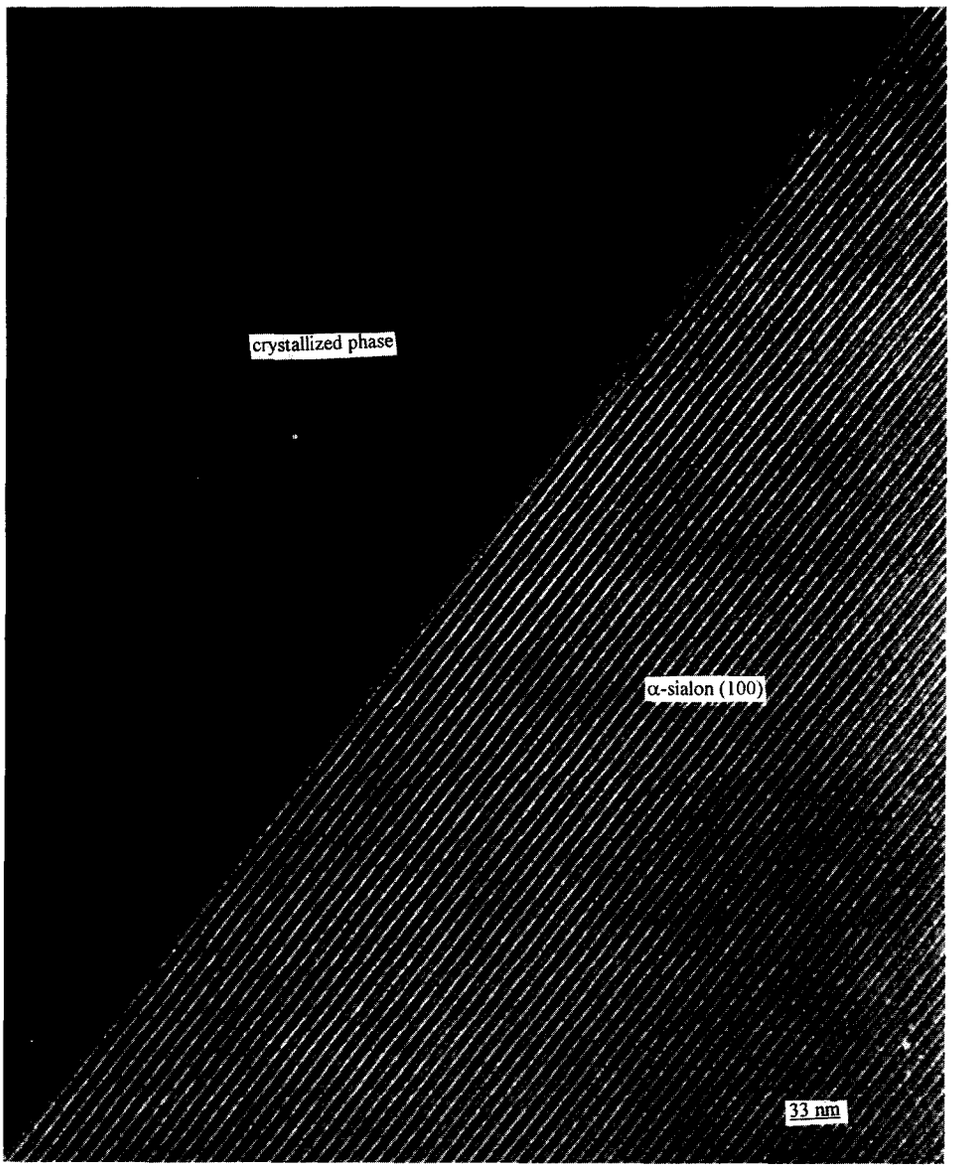

Fig. 9. High resolution transmission electron microscopy micrograph of a cyclic fatigue tested sample of the α'-β'-Sialon material showing complete crystallization of amorphous phases at a triple grain junction.

under large applied stress, it would lead to local deformation and a number of dislocations within grains as shown in Figs 5 and 6. Microscopic results indicated that, in the present material, a crystallization process of the amorphous phase by cyclic fatigue loading will increase the role of dislocation plasticity during high-temperature fatigue fracture.

4.3 The role of creep damage at 1200°C

In brittle materials containing a residual amorphous phase, nonlinear deformation processes such as viscous flow of the intergranular glass films can occur above the glass transition temperature (i.e. the temperature at which the glass becomes viscous). Grain boundary sliding and cavitation accommodate the strains at the crack-tip regions and reduce the stress intensity. Such processes lead to subcritical crack growth at high temperatures in liquid-phase-sintered materials.[26] Although a number of grain boundary phases had been crystallized by the GPS method and applied fatigue stress in the present material at high temperature, some of them unavoidably existed in the form of residual amorphous phase as shown in Fig. 10. Therefore, the above creep deformation mechanisms such as cavity and microcracks may be responsible for certain damage in the present material. Creep damage was commonly observed at a microscopic scale in the form of cavitation. A large number of cavities at multigrain junctions were observed in static fatigue specimens. The content of cavitation was not quantified, but it was merely identified to show that a creep damage mechanism was active in the present study. While it is not known why certain mechanisms are activated or suppressed in cyclic loading, it is observed in the present experiments that cavitation is less prevalent.

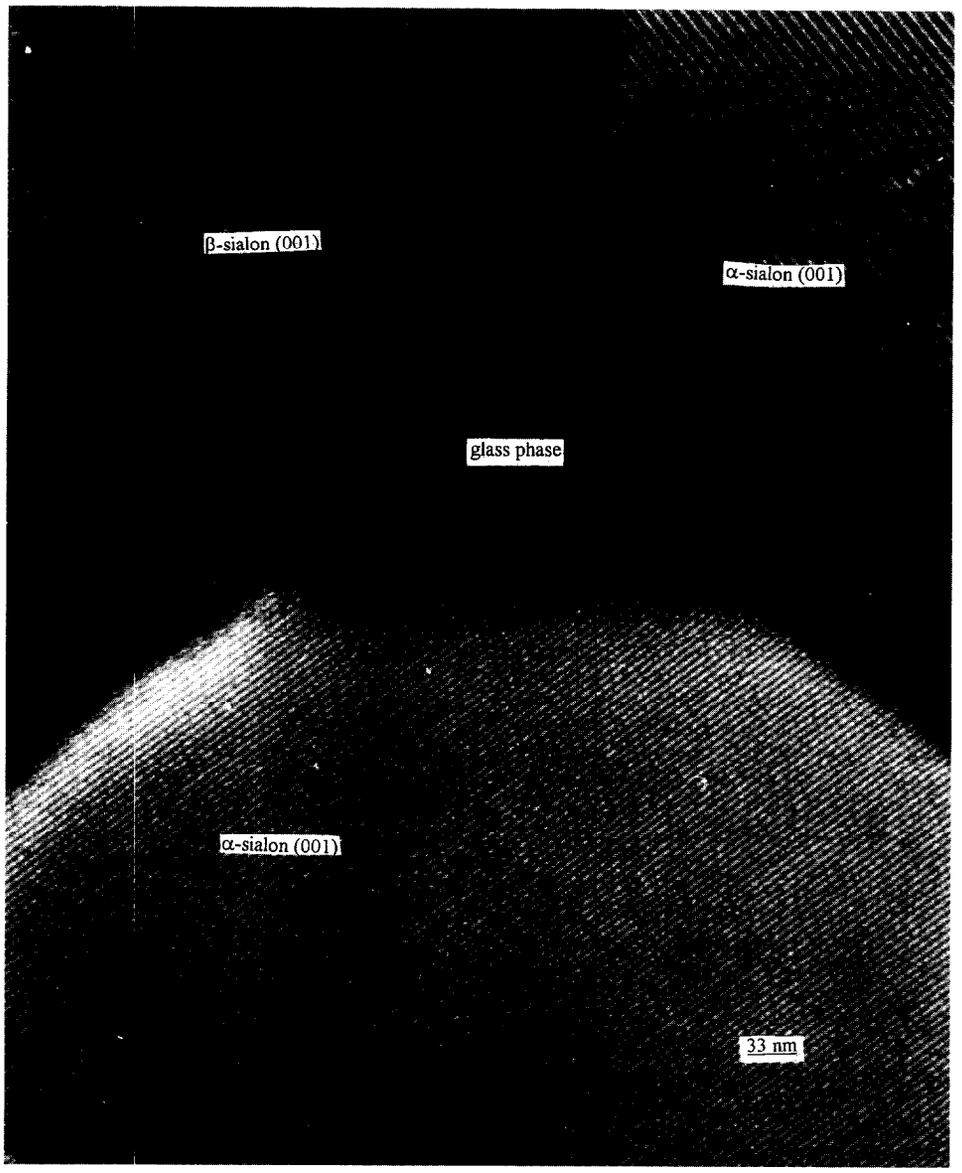

Fig. 10. High resolution transmission electron microscopy micrograph of an as-tested sample of the α'-β'-Sialon material showing amorphous phases at a triple grain junction.

5 Conclusion

Based on a study of static and cyclic fatigue crack growth behaviour from Vickers indentation in Y-α'-β'-Sialon at 1200°C in air, the following conclusions can be drawn:

(1) An effective test method by multiple controlled Vickers flaws in four-point bending configuration was developed for measuring the whole stages of crack growth rate in fatigue testing of structural ceramics at high temperatures.
(2) Similar to ambient temperature fatigue crack growth behaviour in Si_3N_4, the high-temperature static and cyclic fatigue crack growth rates showed three characteristic regions having a plateau with a lowest Paris exponent. At lower stress intensities, cyclic fatigue crack growth rate was slower than that of static fatigue with the same stress intensity factor. At higher stress intensities, the crack growth rates, both static and cyclic fatigue, were almost the same.
(3) In addition to high temperature, the fatigue stresses help aid the crystallization process of amorphous phase and lead to increase of the role of dislocation plasticity during high-temperature fatigue fracture.
(4) In addition to the subcritical crack growth of the main crack, which is assisted by the crack oxidation, a creep damage mechanism such as cavity formation and microcracks may be responsible for static fatigue crack growth in the present study. However, it is not significant for cyclic fatigue.

Acknowledgements

The authors wish to thank Mei-Ling Ruan for TEM and HRTEM and Zeng-Lan Lu for high-temperature fatigue tests. G.-D. Zhan was supported in part by Chinese Post-Doctoral Science Foundation. Also, we wish to thank Dr M. J. Reece and Dr F. Guiu in the Department of Materials, Queen Mary and Westfield College, University of London, for helpful discussions.

References

1. Helms, H. E., Johnson, R. A. and Groseclose, L. E., AGT 100-advanced gas turbine technology developed project. In *Proc. 23rd Automotive Technology Development Contractors' Coordination Meeting*, Series Number P-165. Society of Automotive Engineers, Warrendale, PA, 1986, pp. 137–155.
2. Weiderhorn, S. M. and Fuller, Jr E. R., Structural reliability of ceramics materials. *Mater. Sci. Eng.*, 1985, **71**, 169–186.
3. Jenkins, M. G., Ferber, M. K. and Jack Lin, C.-K., Beneficial effects of cyclic tensile loading on the fatigue resistance of an Si_3N_4. *J. Mater. Sci. Lett.*, 1993, **12**, 1940–1944.
4. Jack Lin, C.-K., Jenkins, M. G. and Ferber, M. K., Tensile dynamic and static fatigue relations for a HIPed silicon nitride at elevated temperatures. *J. Europ. Ceram. Soc.*, 1993, **12**, 3–13.
5. Quinn, G. D., Fracture mechanism maps for advanced structural ceramics. Part 1: Methodology and hot-pressed silicon nitride results. *J. Mater. Sci.*, 1990, **25**, 4361–4376.
6. Quinn, G. D., Fracture mechanism maps for advanced structural ceramics. Part 2: Sintered silicon nitride. *J. Mater. Sci.*, 1990, **25**, 4377–4392.
7. Jack Lin, C.-K., Jenkins, M. G. and Ferber, M. K., Cyclic fatigue of HIPed silicon nitride at elevated temperatures. *J. Mater. Sci.*, 1994, **29**, 3517–3526.
8. Chuck, L., McCullum, D. E., Hecht, N. L. and Goodrich, S. M., High-temperature tension-tension cyclic fatigue for an HIPed silicon nitride. *Ceram. Eng. Sci. Proc.* 1991, **12**(7–8) 1509–1523.
9. Zhan, G.-D., Shi, J.-L., Lai, T.-R., Yen, T.-S., Zhou, Y. and Zhang, Y.-Z., Cyclic fatigue crack propagation in SiCw/Y-TZP Composites: Long and small crack behavior. *J. Mater. Sci.*, 1996, **31**, in press.
10. Zhan, G.-D., Shi, J.-L., Jiang, D.-Y., Wu, F.-Y., Lai, T.-R. and Yen, T.-S., The effect of crystallization of the grain boundary phase on ambient temperature short fatigue crack-growth behavior in Y-α'-β'-Sialon. *J. Mater. Sci.* 1996, **31**, in press.
11. Krohn, D. A. and Hasselman, D. P. H., Static and cyclic fatigue behaviour of a polycrystalline alumina. *J. Am. Ceram. Soc.*, 1972, **55**(4) 208–211.
12. Kosswsky, R., Cyclic fatigue of hot-pressed Si_3N_4. *J. Am. Ceram. Soc.*, 1973, **56**(10), 531–555.
13. Ko, H. N., Fatigue strength of sintered Al_2O_3 under rotary bending. *J. Mater. Sci. Lett.*, 1986, **63**(5), 464–466.
14. Zelizko, V. and Swain, M. V. Influences of surface preparation on the rotating flexural fatigue of Mg-PSZ. *J. Mater. Sci.*, 1988, **23**, 1077–1082.
15. Takatsu, M., Ohya, K. and Ando, M., The relationship between cyclic fatigue properties and microstructure of silicon nitride ceramics. *J. Jpn. Ceram. Soc.*, 1990, **98**(5), 490–498.
16. Dauskardt, R. H., Marshall, D. B. and Ritchie, R. O., Cyclic fatigue-crack propagation in magnesia-partially-stabilized zirconia ceramics. *J. Am. Ceram. Soc.*, 1990, **73**(4), 893–903.
17. Reece, M. J., Guiu, F. and Sammur, M. F. R., Cyclic fatigue crack propagation in alumina under direct tension-compression loading. *J. Am. Ceram. Soc.*, 1989, **72**(2), 348–352.
18. Ritchie, R. O. and Dauskardt, R. H., Cyclic fatigue of ceramics: A fracture mechanics approach to subcritical crack growth and life prediction. *J. Ceram. Soc. Jpn*, 1991, **99**(10), 1047–1062.
19. Guo-Dong Zhan, Toughness and fatigue behavior of particle and whisker-reinforced 3Y-TZP ceramic composites. PhD Dissertation, Huazhong University of Science and Technology, China, 1993.
20. Okazaki, M., McEvily, A. J. and Tanaka, T., On the mechanism of fatigue crack growth in silicon nitride. *Metall. Trans.* 1991, **22A**, 1425–1434.
21. Liu, S.-Y. and Chen, I.-W., Fatigue of yttria-stabilized zirconia: II, Crack propagation, fatigue striations, and short-crack behavior. *J. Am. Ceram. Soc.*, 1991, **74**(6), 1206– 1216.
22. Dauskardt, R. H., James, M. R., Porter, J. R. and Ritchie, R. O., Cyclic fatigue-crack growth in a SIC-whisker-reinforced alumina ceramic composite: Long and small crack behavior. *J. Am. Ceram. Soc.*, 1992, **75**(4), 759–771.
23. Horibe, S., Fatigue of silicon nitride ceramics under cyclic loading. *J. Europ. Ceram. Soc.*, 1990, **6**, 89–95.
24. Mutoh, Y., Yamaishi, K., Miyahara, N. and Oikawa, T., Brittle-to-ductile transition in silicon nitride. In *Fracture Mechanism of Ceramics*, vol. 10, ed. R. C. Bradt *et al.* Plenum Press, New York, 1992, pp. 427–440.
25. Ramamurty, U., Kim, A. S., Suresh, S. and Petrovic, J. J., Micromechanisms of creep-fatigue crack growth in silicon-matrix composite with SiC particles. *J. Am. Ceram. Soc.*, 1993, **76**, 1953–1964.
26. Ramamurty, U., Suresh, S. and Petrovic, J. J., Effect of carbon addition on elevated temperature crack growth resistance in (Mo, W)Si_2–SiC_p Composite. *J. Am. Ceram. Soc.*, 1994, **77**, 2681–2688.
27. Cinibulk, M. K. and Thomas, G., Grain-boundary phase crystallization and strength of silicon nitride sintered with a YSiAlON glass. *J. Am. Ceram. Soc.*, 1990, **73**, 1606–1612.
28. Han, L. X. and Suresh, S., High-temperature failure of an alumina-silicon carbide composite under cyclic loads: Mechanisms of fatigue-crack tip damage. *J. Am. Ceram. Soc.*, 1989, **72**, 1233–1238.
29. Liu, S. Y., Chen, I.-Y. and Tien, T. Y., Fatigue crack growth of silicon nitride at 1400°C: A novel fatigue-induced crack-tip bridging phenomenon. *J. Am. Ceram. Soc.*, 1994, **77**, 137–142.
30. Ewart, L. and Suresh, S., Elevated temperature crack growth in polycrystalline alumina under static and cyclic loads. *J. Mater. Sci.*, 1992, **27**, 5181–5191.
31. Marshall, D. B. and Lawn, B. R., Flaw characteristic in dynamic fatigue: The influence of residual contact stresses. *J. Am. Ceram. Soc.*, 1980, **63**, 532–536.
32. Newman, Jr J. C., and Raju, I. S., Analyses of surface crack in finite plate under tension or bending loads. NASA Technical Paper 1578 (available from National Technical Information Service, Springfield, VA) 1979.
33. ASTM Standard E.740-80, *Standard Recommended Practice for Fracture Testing with Surface-Crack Tension Specimens*. ASTM Annual Book of Standards, vol. 3.01, American Society of Testing and Materials, Philadelphia, PA, 1983, pp. 740–750.